NASA TECHNICAL NOTE

NASA TN D-2652

NASA TN D-2652

STRUCTURAL AND MATERIALS INVESTIGATION OF A 1/8-SCALE-MODEL SPACE STRUCTURE OF TOROIDAL CONFIGURATION AND FILAMENTARY CONSTRUCTION

by Jerry G. Williams and George P. Goodman

Langley Research Center

Langley Station, Hampton, Va.

NATIONAL AERONAUTICS AND SPACE ADMINISTRATION • WASHINGTON, D. C. • FEBRUARY 1965

NASA TN D-2652

STRUCTURAL AND MATERIALS INVESTIGATION OF A 1/8-SCALE-MODEL SPACE STRUCTURE OF TOROIDAL CONFIGURATION AND FILAMENTARY CONSTRUCTION

By Jerry G. Williams and George P. Goodman

Langley Research Center
Langley Station, Hampton, Va.

NATIONAL AERONAUTICS AND SPACE ADMINISTRATION

For sale by the Office of Technical Services, Department of Commerce,
Washington, D.C. 20230 -- Price $2.00

STRUCTURAL AND MATERIALS INVESTIGATION OF A 1/8-SCALE-MODEL SPACE STRUCTURE OF TOROIDAL CONFIGURATION AND FILAMENTARY CONSTRUCTION

By Jerry G. Williams and George P. Goodman
Langley Research Center

SUMMARY

A structural and materials investigation has been conducted on a 1/8-scale model of a proposed 30-foot-diameter torus space structure. Structural design of the model is based on the isotensoid concept in which filamentary material is wound in the torus meridional plane and oriented to carry primary radial structural loads as constant tension in the filaments. Inner and outer equatorial bands provide strength in the circumferential direction. Tests were performed on the model to determine dimensional stability, filament load distribution, hypervelocity impact, and structural failure.

Test results indicated that the overall height of the meridian-plane cross section and the inner and outer diameters increased approximately linearly as the pressure was increased up to 56.0 psi. Strain-gage values of filament loading were approximately 18 percent less than theoretical values for the design operating pressure of 56.0 psi. Failure of the torus occurred at an internal pressure of approximately 94.0 psi, which is approximately 34 percent of the design load based on ultimate strength of the filaments. Structural failure was a result of separation of adjacent torus filaments and not of failure of the filaments themselves.

Author 1

INTRODUCTION

Proposed space vehicles for manned orbital flights have included inflatable structures constructed of flexible materials. Such structures, when deflated, can be packaged into small payload volumes and shapes compatible with the capabilities of available launch vehicles. Upon being placed in orbit the packaged structure is expanded to the desired configuration.

An investigation has been conducted at the Langley Research Center to study structural and materials problems associated with the application of a filament-wound torus as an inflatable spacecraft capable of supporting two men in a low earth orbit for protracted periods of time. A toroid having an inner diameter of 16 feet and an outer diameter of 30 feet was the selected configuration. A 1/8-scale model was constructed for experimental evaluation.

Tests were performed on the model to determine dimensional stability, filament load distribution, hypervelocity impact, and structural failure. Samples of the same basic filament-elastomer material composite as employed in the construction of the torus model were tested for tensile strength.

SYMBOLS

A	torus cross-sectional area
ds	length of element
$d\varphi$	tangential angle of element in meridian plane
h	band width
i	integer
K	characteristic parameter of torus
n	total number of filaments
p	internal pressure of torus
r	distance of element from axis of revolution
T	tension in filament
X,Y,Z	torus axes
α	angle of meridional cusp
δ	angle between adjacent filaments in circumferential plane
θ	angle in circumferential plane
ρ	radius of curvature of element

Subscripts:

c	circumferential
m	meridional
o	equatorial reference
z	axis of revolution

DESCRIPTION OF MODEL AND MATERIALS SPECIMENS

1/8-Scale-Model Torus

Structural design of the 1/8-scale-model torus is based on the concept of optimal use of filamentary material. This design is achieved by orienting the filaments to carry loads in uniform tension. A photograph of the completed torus is presented as figure 1, and sketches showing filament orientation and model dimensions are given in figure 2. Inner and outer diameter dimensions were 24.8 and 45.0 inches, respectively. The maximum dimension perpendicular to the equatorial plane was 10.8 inches. Values of the distance from the rotational axis of symmetry r_z are tabulated and correspond to values of the meridional radius of curvature ρ_z. Design equations for the meridional contour and filament distribution are derived in appendix A. Clusters of circumferential polyester (hereinafter designated PET) filaments were located on the inner and the outer equatorial circumferences to carry circumferential loads perpendicular to the meridional plane. Strength requirements for the equatorial bands are derived in appendix B. Meridional and circumferential filaments were embedded in a nonstructural polyurethane elastomer matrix. The elastomer matrix served to prevent abrasion of filaments, to help pressure seal the inflatable structure, and to allow flexibility of the composite material. The scale-model torus was constructed under contracts to the Langley Research Center.*

Filament winding techniques were employed to fabricate the model of type 52-1100 denier PET filament and a polyurethane elastomer matrix. This filament had an average diameter of 0.013 inch. Based on preliminary tests conducted on both dry and elastomer-impregnated, laminated, cylindrical bands, the design strength of the filament was taken to be 12.5 pounds per filament.

The design operating pressure of the 1/8-scale model corresponded to a full-scale-model operating pressure of 7.0 psi. Since the tensile stress in the torus filaments is a linear function of the torus radius, multiplying by the scale factor of 8.0 gave a model internal operating pressure of 56.0 psi. Applying a safety factor of 5.0 gave a design burst pressure for the 1/8-scale model of 280 psi. This design procedure resulted in a wall thickness and strength equivalent to that of the full-scale model. The composite filament-elastomer material weighed 0.25 psf.

The toroidal shell consisted of 12,800 meridional turns of type 52-1100 denier PET filament applied in four layers of approximately 3200 turns. The first and last layers were impregnated with a polyurethane elastomer and the two middle layers were applied dry (without elastomer). Meridional filaments at the outer equator were continuously spaced with 90 filaments per inch. Meridional filaments converged toward the rotational axis of symmetry of the torus with a resulting filament distribution of 164 filaments per inch at the inner equator.

---

*Astro Research Corporation, P.O. Box 4128, Santa Barbara, California, Contracts NAS1-889 and NAS1-1078.

Detailed sketches of the equatorial bands required to carry loads perpendicular to the meridian plane are shown in figure 3. The outer band consisted of a cluster of 1270 circumferential turns of dry type 52-1100 denier PET filaments. Filaments were held in place by short transverse strips of polyurethane elastomer applied at approximately 2-inch intervals. Approximately 100 turns of the outer band were inside of the meridian winding and the remaining turns were outside.

The inner band was composed of 634 turns of type 52-1100 denier PET filament and was located on the inner toroidal circumference in the equatorial plane, inside of the meridional windings. The inner band was 1.4 inches in width and was built up from seven individual concentric bands. Each band was approximately 0.020 inch in thickness and was sandwiched between two layers of 1-mil-thick poly[ethylene terephthalate] (designated PET) film. The entire inner band was sheathed in a 1-mil-thick, contact adhesive coated, aluminized PET tape.

The derivation of the equations necessary to determine the number of meridional and circumferential windings required to obtain a design burst pressure of 280 psi is given in appendix B.

A double layer of 1-mil-thick, contact adhesive coated, PET tape (fig. 4) was used to form an inner leak-proof liner. Residual leakage of the liner was prevented by slosh coating the adhesive tape liner with rubber fluid sealant. A single layer of contact adhesive coated, aluminized PET tape was used to form a nonsealing external protective sheath for the complete torus assembly (fig. 1). This layer was removed for the experimental tests.

To facilitate pressurization, a basketball valve was located on the outer equatorial band. Construction and installation details are shown in figure 5. Rubber disks which support the valve were located inside and outside the inner PET liner. A small threaded plug provided for positive closure of the valve.

A component weight breakdown is given in table I. Total weight of the 45-inch-diameter isotensoid torus was 8.38 pounds.

Tension Band Specimens

Tension test specimens of the composite material, PET filament and polyurethane elastomer, were circular bands 1 inch wide and 8 inches in diameter. Descriptive data for the three specimens tested are given in table II. The bands were constructed by wrapping a continuous PET filament (type 52-1100 denier) around an 8-inch-diameter mandrel. Brush coatings of polyurethane elastomer were applied to the PET filaments as wrapping progressed. Each test specimen consisted of 100 turns of PET filament to yield a 1-inch-wide band. The cross-sectional area of each band was 0.0136 square inch. The cross-sectional area of polyurethane elastomer contained in each test band varied as indicated in table II.

TESTS

1/8-Scale-Model Torus

It had been intended to conduct folding and packaging tests on the model. However, because of the unexpected stiffness of the inner leak-sealing liner, the model was not as flexible as originally intended, and the tests were not conducted. Other investigations have shown that filament-wound structures of equivalent strength and ability to retain pressure were adequately flexible for packaging. (See, for example, ref. 1.) Improved sealing methods and modified construction techniques involving the limited use of a low modulus binder, the prevention of filament saturation, and the inclusion of a moderate twist in the filaments can result in the required flexibility.

Dimensional stability.- Dimensional stability tests consisted of determining the variation of the physical dimensions of the 1/8-scale-model torus at various inflation pressures up to the operating pressure of 56.0 psi. The test setup used in the dimensional stability tests is shown in figure 6. Inflation pressure was indicated by a calibrated 16-inch-dial pressure gage. Outside-equatorial-diameter and inside-equatorial-diameter measurements were made with an outside caliper and an inside micrometer, respectively. A height gage, with the surface plate as a base reference, was used to measure the maximum dimension (in the meridian plane) perpendicular to the equatorial plane. The shape of the torus cross section, in the meridian plane, was visually compared with a template constructed by use of calculated dimensions.

Initial measurements of the outside equatorial diameter, inside equatorial diameter, and maximum dimension (in the meridian plane) perpendicular to the equatorial plane were made at an inflation pressure of 15.0 psi. The variation of dimensions with inflation pressure was obtained by means of dial gages located as shown in figure 6, which indicated the changes in these dimensions as inflation pressure was increased from 15.0 psi.

To determine the angular displacement of the outer equatorial band with respect to a plane perpendicular to the torus equatorial plane (or surface plate), two dial gages separated by a vertical distance of $2\frac{5}{8}$ inches were positioned in a meridional plane as indicated in figure 6. One gage was located at the upper edge of the outer band and the other at the lower edge of the outer band. Dial gage indications were recorded for several values of inflation pressure from the inflation pressure of 15.0 psi to the scale operating pressure of 56.0 psi. These measurements were compared with the initial measurements obtained at 15.0 psi in order to determine the angular displacement of the outer equatorial band.

Load distribution.- Load distribution of the composite PET-polyurethane torus material was experimentally measured by resistance strain gages for several values of inflation pressure. Strain gages were located in a meridian plane and positioned around the external periphery of the torus meridional cross section as shown in figure 7. Strain gages 1 to 12 were regular foil

gages (gages of etched foil filaments made from a constantan alloy) and gages 13 to 18 were postyield gages. The postyield gages were located diametrically opposite foil gages 1 to 6 and parallel to foil gages 7 to 12. Postyield gages were used because of their effectiveness in measuring large strains and these measurements were compared with foil-gage recordings of strain. All strain gages were bonded to the torus with polyurethane cement, the torus elastomer material. Strain gages 1 to 5, 7 to 11, and 13 to 17 measured strain along the meridian; gages 6, 12, and 18 measured strain circumferentially along the outer equatorial band.

Inflation of the torus to various values of internal pressure was manually controlled by a pressure reducing valve and a calibrated 16-inch-dial pressure gage. Strain measurements were recorded for the various inflation pressures, which began at 15.0 psi, by systematically (without time lapse) increasing the pressure in 5.0 psi increments to a pressure of 50.0 psi. Strain measurements were also recorded for the design operating pressure of 56.0 psi and for the deflation in 5.0 psi increments from 50.0 to 15.0 psi. The entire test was performed twice.

To obtain a calibration between the recorded torus strains and the torus load per filament, a meridional section cut from the torus was calibrated with static dead loads. The section was composed of 90 filaments and varied in width because of the radial effect of a meridionally wound torus from 1.0 inch at the outer circumference to 0.547 inch at the inner circumference. Since this was a static load test, loads were applied to both sides of the section and, consequently, equally distributed among the 180 filaments (90 per side). Strain gages of constantan alloy wire formed in a strain-sensitive 6-inch-long grid were mounted on both sides of the narrow band. The zero-reference strain corresponded to a static load of 50 pounds. The band was stressed by applying dead load weights in increments of 100 pounds up to a total load of 450 pounds. Corresponding strains were recorded.

Hypervelocity impact.- A hypervelocity impact test of the inflated 1/8-scale-model torus was made in the hypervelocity impact laboratory at the Langley Research Center. The 1/8-scale-model torus was inflated to the scale operating pressure of 56.0 psi for this test. Stresses in the 1/8-scale-model wall material at this pressure are equal to stresses in the full-scale-torus wall material at an operating pressure of 7.0 psi.

Figure 8(a) is a schematic of the 1/8-scale-model-torus hypervelocity-impact test setup. A helium gun fired into a vacuum chamber was employed to propel a 1/16-inch-diameter spherical copper projectile. A description of the gun and the technique for measuring projectile velocity are given in reference 2. The projectile, fired into the vacuum chamber, traversed the length of the vacuum chamber, ruptured a PET diaphragm covering the vacuum chamber port, and traveled approximately 3 feet through the atmosphere before impacting the target. The equatorial plane of the 1/8-scale-model torus was perpendicular to the projectile path. Figure 8(b) is a photograph of the 1/8-scale-model-torus hypervelocity-impact test setup. Vacuum-chamber pressure for this test was 2 mm of mercury. Two holes were made in the torus by the projectile. Following the conclusion of the hypervelocity impact test, the two resulting holes were sealed in preparation for the structural failure test.

Structural failure.- The maximum inflation pressure which could be retained by the 1/8-scale-model torus without structural failure was determined by increasing the inflation pressure until a structural failure occurred. The test setup was essentially the same as that shown in figure 6. Inflation pressure was measured by a 16-inch-dial pressure gage. Strain gages were disconnected from the recorder and dial gages were removed for this test.

Tension Bands

The tensile breaking load and elongation as a function of load data for the PET-polyurethane tension specimens were obtained by use of the tensile testing instrument (see ref. 3) at the Langley Research Center. Figure 9 shows a tension test band mounted on adapted spool fittings. Three tensions bands were tested to the breaking load. The rate of loading for the tension test bands was 0.05 inch per minute. A 5-inch gage length was marked on each test band at near zero load for use in determining elongation as a function of load. Elongation of the 5-inch gage length, as tension load increased, was determined by comparing the elongated gage length with dividers preset at given distances for values representing 2-percent intervals of elongation. At each 2-percent elongation interval a tick mark was made on a permanent chart by manual control of the recording stylus provided on the test equipment.

RESULTS AND DISCUSSION

1/8-Scale-Model Torus

Dimensional stability.- Measured physical dimensions of the 1/8-scale-model torus, when the torus was inflated to 15.0 psi, were as follows:

Outer equatorial diameter, in.	45.08
Inner equatorial diameter, in.	24.80
Height in meridian plane, perpendicular to equatorial plane, in. . . .	10.65

Comparison of the measured dimensions with design dimensions of the 1/8-scale-model torus shown in table III indicates that the 1/8-scale filament-wound torus was fabricated with reasonable accuracy. The shape of the meridional-plane cross section of the 1/8-scale-model torus appeared to be in close agreement with a template constructed by use of design dimensions. The dimensions defining the shape of the meridional cross section are shown in figure 2.

Variation of the outer equatorial diameter with increasing inflation pressure is shown in figure 10(a). The variation was approximately linear from 45.08 inches at 15.0 psi to 45.33 inches at the design operating pressure of 56.0 psi. The variation of the inner equatorial diameter with increasing inflation pressure was also approximately linear, as shown in figure 10(b). Variation of the maximum dimension in the meridian plane (perpendicular to the equatorial plane) with increasing inflation pressure is shown in figure 10(c) and is approximately linear.

The variation of angular displacement of a region of the outer equatorial band with increasing inflation pressure is shown in figure 10(d). The angular displacement referenced to a plane perpendicular to the torus equatorial plane increased approximately linearly to a maximum of 0.8° with increasing inflation pressure up to a maximum of 56.0 psi. This relationship suggests that torus instability might occur at higher inflation pressures. However, to define completely the torus angular displacement, additional information would be required concerning the angular displacement of several regions on the torus periphery and at higher inflation pressures. The manufacturer recommends, in order to prevent the angular displacements that accompany pressurization of a meridionally wound torus, that the isotensoid filaments be wound in a counter-rotating double helix pattern.

Load distribution.- Figure 11 is a record of the strain for static loading of the 90-filament-wide section cut from the 1/8-scale-model torus. Note that the zero strain is for an initial load of 50 pounds. The two strain gages (with 6-inch-long grid) placed on the section recorded slightly different values of strain. For calibration purposes, the slope of a straight line drawn through an average of the two values was taken. A set in the material is indicated by the nonzero value of strain observed for the unloading cycle of the torus section. However, after approximately 1 hour, a zero strain was recorded for the 50-pound load.

Values for strain gages 1, 7, and 13 (r_z = 18.13 in.) for various pressures up to 56.0 psi are shown in table IV. An average value of strain was calculated from the three strain gages and included two tests per gage for each pressure. The load corresponding to each average strain was determined for a 180-filament band by using the slope of the calibration curve of figure 11. Filament loading was not tabulated for strain gages 6, 12, and 18 because these gages were located on the torus circumference; thus direct correlation was questionable. The torus load per filament is given as a function of internal pressure in figure 12. The relationship is approximately linear. Since the experimental zero value of strain corresponded to 15.0 psi, the 0 to 15.0 psi region of the graph was defined by extrapolating a straight line with the same slope as in the 15.0 to 56.0 psi region of the graph. Thus defined, the 15.0 psi pressure load was 0.56 pound per filament. The theoretical isotensoid values of load are also presented in figure 12. Comparison shows that the experimental results are approximately 18 percent less than the theoretical isotensoid values.

Several torus strain-gage measurements for two experimental tests at the design operating pressure of 56.0 psi are given in table V. Values of strain recorded by regular foil strain gages compare favorably with those recorded by postyield strain gages. Strains were recorded in microinches per inch and the load corresponding to each strain was determined for a 180-filament band by using the slope of the calibration curve of figure 11. Since the zero strain measurement corresponded to 15.0 psi pressure, the extrapolated value of strain for the 15.0 psi pressure of 0.56 pound per filament was added to the strain determined load to obtain the total torus load per filament.

In figure 13, the average experimental load per filament (average of two tests and three strain gages per test) and the theoretical isotensoid load per filament for the torus at an internal pressure of 56.0 psi are plotted against r_z, the distance of the strain gages from the torus axis of revolution. All results are within approximately 0.1 pound of 2.0 pounds per filament which is approximately 81 percent of the theoretical isotensoid load of 2.47 pounds per filament. Close agreement of filament load calculated from strain-gage measurements, particularly between measurements from gages 1, 7, and 13 and gages 4, 10, and 16, which are equidistant from the axis of revolution but diametrically on opposite sides of the torus, indicates that the filaments were indeed loaded according to isotensoid design.

Several factors could contribute to the differences observed between theoretical isotensoid and measured loads per filament. Some inaccuracy may have been introduced in the calibration relating strain-gage measurements to filament load. The strain-gage cement and the polyurethane matrix may have offered some resistance to strain, particularly in view of the short time interval between test measurements at the various pressures. Close agreement between the toroid model (pressurized to 15.0 psi) and the design geometry indicates that construction errors did not contribute significantly to the difference in filament load. However, with regard to design geometry, some refinement could possibly be made through a consideration of boundary conditions at the discontinuity indicated by the theory (see appendix A) at the inner and outer circumferential bands.

Hypervelocity impact.- Closeups of the holes made in the wall material of the 1/8-scale-model torus by the 1/16-inch-diameter spherical copper projectile are shown in figure 14. Projectile velocity was 10,600 fps prior to impact and was measured approximately 1 foot from the torus target area. An exterior view of the projectile entrance hole is shown in figure 14(a). The diameter of the hole is approximately 1/8 inch. Several filaments were severed and separated from the elastomer for a length of approximately 1/2 inch as indicated in the photograph.

An exterior view of the hole in the torus wall material made by the emerging projectile is shown in figure 14(b). The properties of this hole are very similar to those of the initial impact hole. The hole is approximately 1/8 inch in diameter. Severed filaments were held in their respective meridian planes by the elastomer matrix, except for a section approximately 3/8 inch adjacent to the hole.

Damage to the torus wall while under full-scale stress conditions was not catastrophic but was of a local nature and confined to the impact and emergence areas. The filament-wound-model torus remained intact and internal pressure was gradually reduced by the leakage of air through the holes.

It should be noted that the projectile velocity was not high enough to cause particle breakup, as evidenced by the single exit hole. If the projectile velocity were sufficiently increased, particle breakup and conical dispersion could cause a different impact phenomenon on the inner wall. Instead of one hole with characteristics similar to the entrance hole, several holes or

even one large hole would probably occur. If the inner wall were sufficiently strong, it possibly could even resist penetration due to the reduced load per unit area effected by the particle dispersion.

Structural failure.- Structural failure of the 1/8-scale-model torus occurred at an inflation pressure of 94.0 psi. This pressure is 33.6 percent of the 280 psi design failure pressure. A photograph of the 1/8-scale-model torus after the structural failure test is presented as figure 15.

Overall failure of the composite filament-wound elastomer structure was the result of numerous local failures which occurred on only one side of the model torus. Local structural failures which could be detected by visual inspection of the model were encircled, as indicated in figure 15. A closeup of a typical failure is shown in figure 16. Inspection of the many local failures indicated that the meridionally wound filaments had been displaced from the meridian plane and that the elastomer matrix and inner liner between meridian filaments had been ruptured. Displaced meridian filaments are shown in figure 16. Close inspection of the local failures revealed no broken meridian filaments.

The occurrence of structural failure on only one side of the model torus is difficult to explain. Perhaps it was a result of less polyurethane elastomer on this side of the torus than on the other as was somewhat evident from inspection, but a satisfactory explanation has not been conjectured. Failure did not occur where the hypervelocity impact hole had been sealed. The low-pressure failure of the matrix indicates that the integrated filament-matrix design of a filament-wound structure is very important. A helix winding pattern in which filaments crisscross and overlap (a characteristic not common with the meridionally wound torus) would probably increase the resistance of the filament-matrix composite to this type of failure. In addition, the matrix strength could be increased by selection of a different elastomer and by better quality control in the elastomer application.

Tension Bands

Tension test data for the composite PET-polyurethane tension test bands are given in table VI. The average breaking load of three tension test bands is 1702 pounds, with an average breaking load per filament of 17.02 pounds. Average ultimate tensile stress based on the PET cross-sectional area is 125,122 psi. Average maximum elongation of the three test bands is approximately 12 percent. Breaks in the material test bands 1 and 3 occurred outside of the 5-inch gage length, whereas the break in band 2 occurred within the 5-inch gage marks.

SUMMARY OF RESULTS

Results of experiments conducted on a 1/8-scale model of an inflatable isotensoid meridionally wound torus may be summarized as follows:

1. Variation with pressure of the outer and inner equatorial diameter and the maximum dimension in the meridional plane (perpendicular to the equatorial plane) is approximately linear.

2. Angular-displacement variation of one region of the outer diameter circumferential band referenced to a plane perpendicular to the torus equatorial plane increased with inflation pressure to a value of 0.8° at the 56.0 psi design operating pressure; this relationship suggested that instability might occur at higher inflation pressures.

3. Filament loading determined from strain-gage measurements was approximately 18 percent less than theoretical isotensoid values corresponding to pressures up to 56.0 psi.

4. Close agreement between filament loading at various locations on the torus at the 56.0 psi design pressure indicates that the filaments were loaded consistent with isotensoid design.

5. Damage to the pressurized 1/8-scale-model torus from the impact of a 1/16-inch-diameter copper sphere at a velocity of 10,600 fps was not catastrophic but was confined to local areas and consisted of a 1/8-inch-diameter hole and a few frayed filaments.

6. Structural failure occurred at an inflation pressure of 94.0 psi which is 33.6 percent of the 280 psi design failure pressure.

7. Failure was the result of numerous local failures due to separation of adjacent filaments on only one side of the torus with a resulting rupture of the inner liner.

8. The composite polyester-polyurethane tension bands were found to have an average tensile strength of 17.02 pounds per filament for the type 52-1100 denier polyester filaments.

A suggested solution to the high-pressure instability problem and the premature matrix failure associated with the meridionally wound torus is construction of the torus in a counterrotating double helix pattern.

Langley Research Center,
National Aeronautics and Space Administration,
Langley Station, Hampton, Va., October 15, 1964.

APPENDIX A

DERIVATION OF DESIGN EQUATIONS FOR ISOTENSOID TORUS

The following design equations for the meridionally wound torus were originally derived by H. U. Schuerch and A. C. Kyser.* Consider a thin shell of revolution, with meridional load carrying filaments subject to a uniform internal pressure p, as shown in figure 17. Let the axis of revolution be the Z-axis and the tension in each meridional filament be denoted by T_m. The total number of meridional filaments is denoted by n_m; ρ_z denotes the radius of curvature for the element at distance r_z from the axis of revolution.

Summing the forces along the meridian (Σ forces = 0) yields

$$p\ ds\ 2\pi r_z = 2T_m n_m \frac{d\varphi}{2}$$

but

$$d\varphi = \frac{ds}{\rho_z}$$

thus,

$$p\ ds = \frac{T_m n_m}{2\pi r_z} \frac{ds}{\rho_z}$$

and

$$\frac{1}{\rho_z} = \frac{2\pi p r_o^2}{T_m n_m} \frac{r_z}{r_o^2} \tag{A1}$$

Solving for T_m gives

$$T_m = \frac{2\pi p}{n_m} \rho_z r_z \tag{A2}$$

Thus, for isotensoid design, that is, equal tension in the filaments, $\rho_z r_z$ must be equal to a constant.

The characteristic torus parameter K can be expressed as

$$K = \frac{2\pi p r_o^2}{T_m n_m}$$

---

*Astro Research Corporation, P.O. Box 4128, Santa Barbara, California, Contract NAS1-889.

Then, from equation (A1)

$$K = \frac{r_o^2}{\rho_z r_z} \tag{A3}$$

and substitution of the particular value

$$\rho_z r_z = \rho_o r_o = \text{Constant}$$

the characteristic torus parameter becomes

$$K = \frac{r_o}{\rho_o}$$

The result is the nondimensional equation

$$\frac{\rho_o}{\rho_z} = \frac{r_z}{r_o}$$

where

K	characteristic torus parameter
ρ_o	radius of curvature of meridian at equator
r_o	equatorial radius
ρ_z	radius of curvature of meridian
r_z	distance of meridian from the axis of rotation
p	internal pressure
n_m	total number of meridional filaments
T_m	tension in each meridional filament

The only value of K in equation (A3) which yields a completely closed-in-itself torus is an unreasonable torus with zero inner radius and lemniscate-type cross section. It is necessary, therefore, to form the meridian of a practical torus-shaped pressure vessel by piecing together several branches of particular solution of equation (A3). Circumferential rings, working in tension alone, can physically supply this solution provided they are located at points of local maximum and minimum values of r_z.

Either of two methods may be utilized to determine the analytic solution to equation (A3). The first method is the column analog solution. A complete discussion of this method can be found in reference 4. The second method of

solution is a graphical solution. This solution is obtained by selecting the desired value of K and tabulating ρ_z against r_z. The resulting relationships can then be used to construct graphically the torus cross section.

APPENDIX B

DERIVATION OF CIRCUMFERENTIAL BAND REQUIREMENTS

The circumferential band requirements necessary to complete the solution described in appendix A can be derived by considering the following equilibrium conditions illustrated in figure 18(a):

$$2n_cT_c = 2\sum_{i=0}^{n_m/2} T_m \cos\frac{\alpha}{2}\sin\theta_i$$

where

$$\theta_i = i\delta$$

and

$$n_m\delta = 2\pi$$

Then

$$n_cT_c = T_m \cos\frac{\alpha}{2}\frac{\sin\frac{n_m\delta}{4}\sin\frac{\left(n_m/2\right)+1}{2}\delta}{\sin\frac{\delta}{2}}$$

$$= T_m \cos\frac{\alpha}{2}\cot\frac{\pi}{n_m}$$

$$\approx T_m \cos\frac{\alpha}{2}\left(\frac{n_m}{\pi} - \frac{1}{3}\frac{\pi}{n_m} - \frac{1}{45}\left(\frac{\pi}{n_m}\right)^3 - \cdots\right)$$

Since $n_m \gg 1$,

$$n_cT_c = \frac{n_mT_m}{\pi}\cos\frac{\alpha}{2} \qquad \text{(B1)}$$

A check for this calculation is provided by considering the condition of equilibrium across a meridional plane through the torus (as shown in fig. 18(b)):

$$n_c T_c = pA \tag{B2}$$

where

A	torus cross-sectional area
n_c	total number of circumferential filaments
p	pressure
T_c	tension in each circumferential filament
$\frac{\alpha}{2}$	half-angle of meridional cusp

The circumferential filaments may be distributed in a wide band on the outer circumference, as shown in figure 18(c). To prevent band filament slippage, the outer band must be located at the outer perimeter to form a cylindrical section of the torus. The filament density required is given by the cylinder hoop-force equilibrium condition

$$h_c r_c p = n_c T_c \tag{B3}$$

where h_c is the circumferential band width. A portion of the circumferential filaments required is usually placed in a band at the inner circumference.

REFERENCES

1. Olson, M. W.: A Research Study To Investigate the Application of Filament Winding for Sections of an Erectable Space Station. Final Rept. (Contract NAS1-2317), U.S. Rubber Co., Apr. 1963.

2. Collins, Rufus D., Jr.; and Kinard, William H.: The Dependency of Penetration on the Momentum Per Unit Area of the Impacting Projectile and the Resistance of Materials to Penetration. NASA TN D-238, 1960.

3. Hindman, Harold; and Burr, G. S.: The Instron Tensile Tester. Trans. ASME, vol. 71, no. 7, Oct. 1949, pp. 789-796.

4. Schuerch, H. U.; Burggraf, O. R.; and Kyser, A. C.: A Theory and Applications of Filamentary Structures. NASA TN D-1692, 1962.

TABLE I.- WEIGHT BREAKDOWN FOR 45-INCH-DIAMETER ISOTENSOID TORUS*

Torus components	Weight of PET filament, lb	Weight of polyurethane elastomer, lb	Weight of sealant and PET tape, lb	Total weight of components, lb
Inner band	0.34	0.13	0.12	0.59
Leakage barrier	----	----	1.12	1.12
Meridional winding	2.95	.83	----	3.78
Outer band	1.42	.11	----	1.53
Outer skin	----	----	.59	.59
Total	4.71	1.07	1.83	7.61

*Additional weight of puncture seal fluid was 0.77 lb.

TABLE II.- DATA FOR TENSION TEST BANDS

Band specimen	Average thickness, in.	Total cross-sectional area, sq in.	Area of PET filament, sq in.	Area of polyurethane elastomer, sq in.	PET-filament area, percent total band area	Polyurethane-elastomer area, percent total band area
1	0.031	0.031	0.0136	0.0174	43.87	56.13
2	0.028	0.028	0.0136	0.0144	48.57	51.43
3	0.023	0.023	0.0136	0.0094	59.13	40.87

TABLE III.- TORUS DIMENSIONAL-STABILITY DATA

Pressure, psi	Outside diameter, in.	Inside diameter, in.	Height in meridional plane perpendicular to equatorial plane, in.	Angular displacement, deg
15.0	45.08	24.80	10.65	0
25.0	45.15	24.82	10.66	0.24
35.0	45.20	24.85	10.68	0.41
40.0	45.23	24.87	10.68	0.51
45.0	45.26	24.88	10.69	0.62
50.0	45.30	24.89	10.70	0.74
56.0	45.33	24.91	10.71	0.80
56.0 (operating pressure for design dimensions)	45.0	24.8	10.75	0

TABLE IV.- TORUS FILAMENT LOAD FOR SEVERAL PRESSURES

Pressure, psi	Torus strain from gage 1, μin./in.	Torus strain from gage 7, μin./in.	Torus strain from gage 13, μin./in.	Average torus strain, μin./in.	Torus load per 180 filaments,[a] lb	Total torus load per filament, lb
15	0 0	0 0	0 0	0	0	0.560
25	1021 924	1021 924	973 924	965	59.81	.892
35	1982 1969	1982 1970	1933 1970	1968	122.00	1.238
40	2529 2492	2517 2493	2456 2481	2495	154.67	1.419
45	3100 3040	3052 3064	2991 3040	3048	189.00	1.610
50	3660 3648	3599 3648	3526 3636	3620	224.46	1.807
56	4426 4158	4353 4170	4268 4147	4254	263.70	2.025

[a]Based on pressure of 15.0 psi (zero strain).

TABLE V.- TORUS FILAMENT LOAD FOR AN OPERATING PRESSURE OF 56.0 PSI

Strain gage	Torus strain, μin./in.	Torus load per 180 filaments,[a] lb	Total torus load per filament, lb
1	4426 4158	274.4 257.9	2.084 1.992
2	4219 4061	261.6 251.8	2.013 1.959
3	4013 3903	248.8 242.0	1.942 1.904
4	3854 3709	238.9 229.9	1.887 1.837
5	3721 3526	230.7 218.6	1.841 1.774
[b]6	4475 4256		
7	4353 4170	269.9 258.7	2.060 1.997
8	4317 4134	267.6 256.3	2.047 1.984
9	3988 3843	247.3 238.3	1.934 1.884
10	4173 3952	258.6 245.0	1.997 1.921
11	3988 3770	247.3 233.7	1.934 1.858
[b]12	3818 3745		
13	4268 4147	264.6 257.1	2.030 1.988
14	4341 4207	269.1 260.8	2.055 2.009
15	4085 3952	253.3 245.0	1.967 1.921
16	4304 4183	266.8 259.3	1.962 2.001
17	4159 4061	257.9 251.8	1.993 1.959
[b]18	4049 3964		

[a]Based on pressure of 15.0 psi (zero strain).
[b]Circumferential.

TABLE VI.- LOAD DATA FOR TENSION TEST BANDS

Band specimen	Total test load, lb	Load per side of band, lb	Elongation, percent	Breaking load per filament, lb	Tensile stress based on area of PET filament, psi
1	25.0	12.5	----------		
	690.0	345.0	2		
	1025.0	512.5	4		
	1470.0	735.0	6		
	2375.0	1187.5	8		
	3170.0	1585.0	10		
	3260.0	1630.0	Break	16.3	119,853
2	40.0	20.0	----------		
	680.0	340.0	2		
	960.0	480.0	4		
	1420.0	710.0	6		
	2390.0	1195.0	8		
	3210.0	1605.0	10		
	3500.0	1750.0	12 (Break)	17.5	128,676
3	15.0	7.5	----------		
	625.0	312.5	2		
	910.0	455.0	4		
	1290.0	645.0	6		
	1940.0	970.0	8		
	2850.0	1425.0	10		
	3430.0	1715.0	12		
	3450.0	1725.0	Break	17.25	126,838

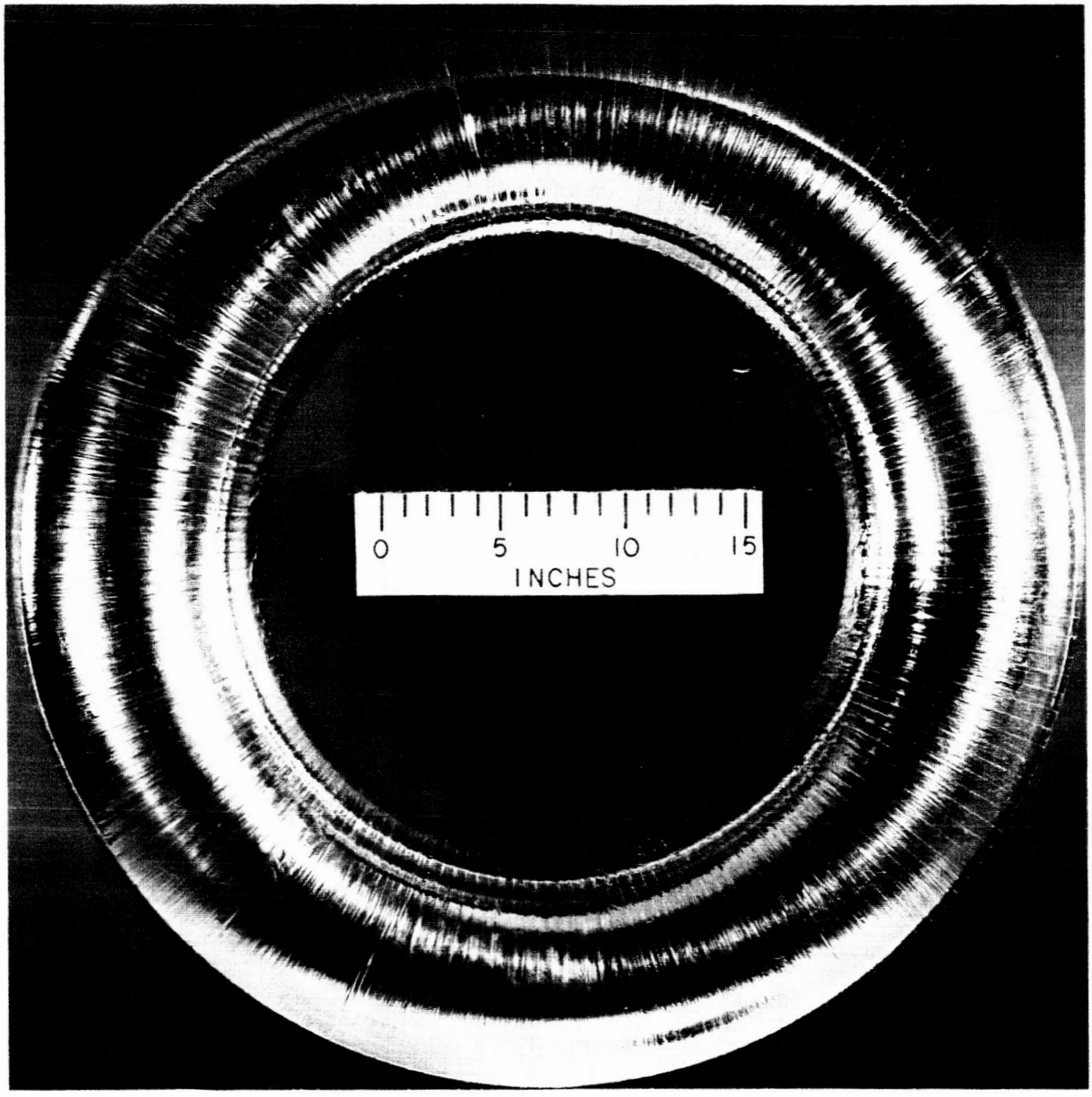

L-61-3579.1

Figure 1.- The 1/8-scale model of isotensoid torus.

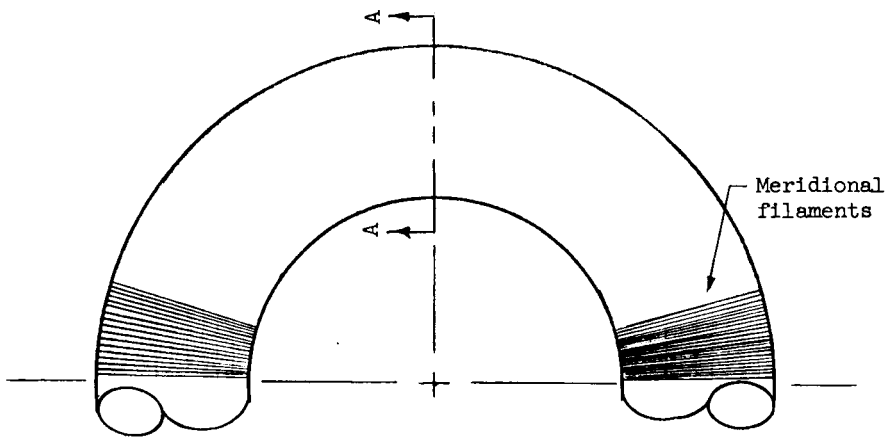

(a) Top view.

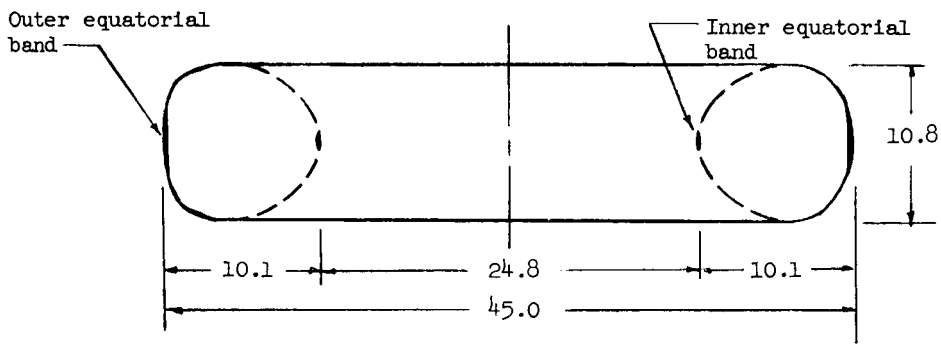

(b) Side view.

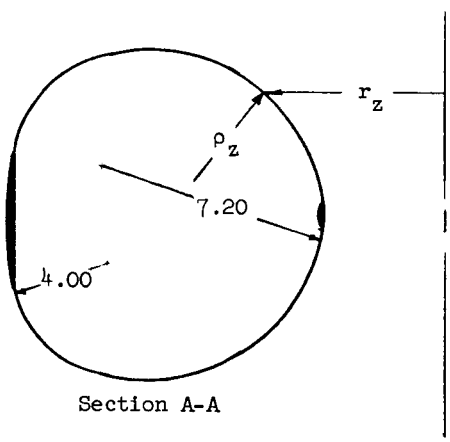

r_z, in.	ρ_z, in.
22.50	4.00
21.50	4.18
20.50	4.39
19.50	4.61
18.50	4.87
17.50	5.14
16.50	5.46
15.50	5.80
14.50	6.21
13.50	6.66
12.50	7.20

(c) Cross-sectional view.

Figure 2.- Dimensional sketch of 1/8-scale-model torus. Dimensions are in inches.

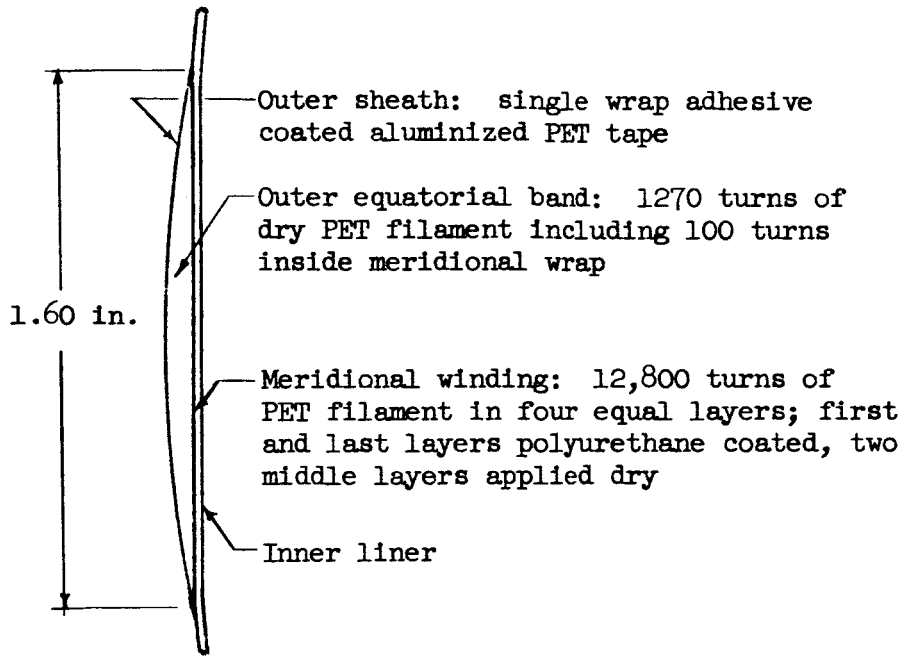

(a) Outer equatorial band.

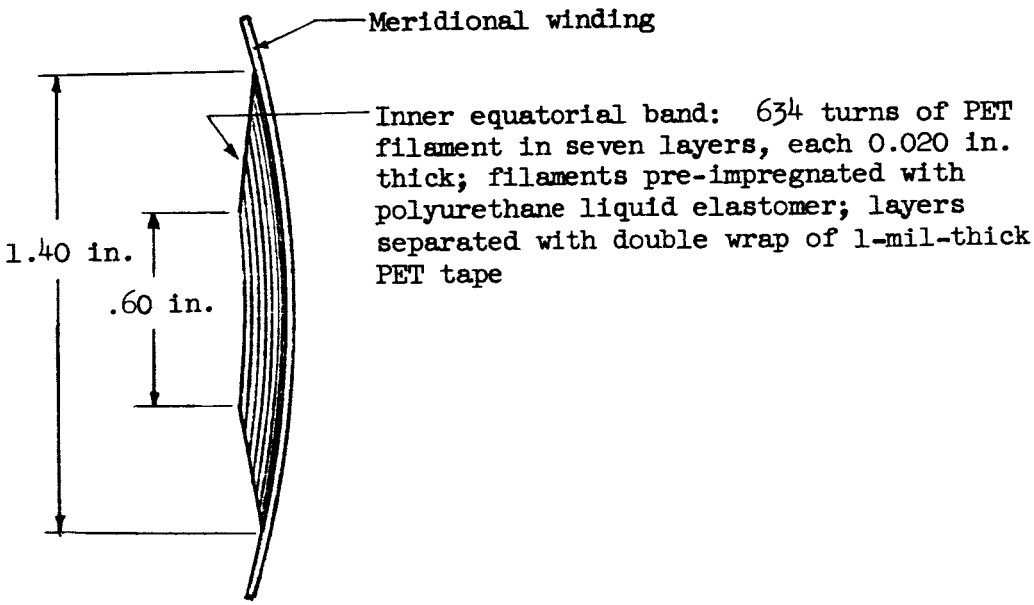

(b) Inner equatorial band.

Figure 3.- Details of inner and outer equatorial band.

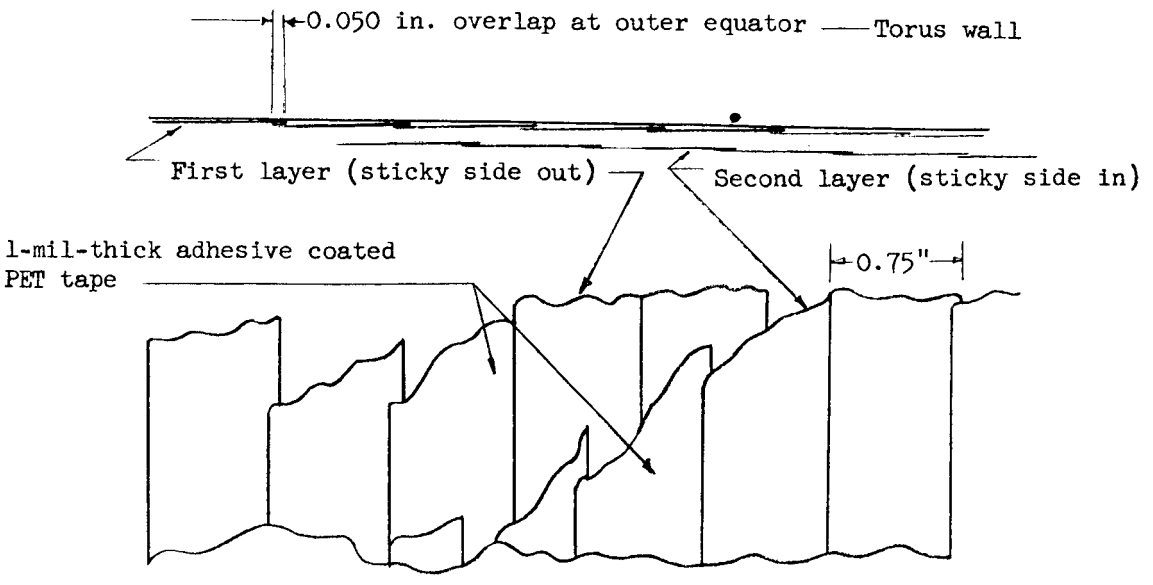

Figure 4.- Sealant-tape-wrapping scheme.

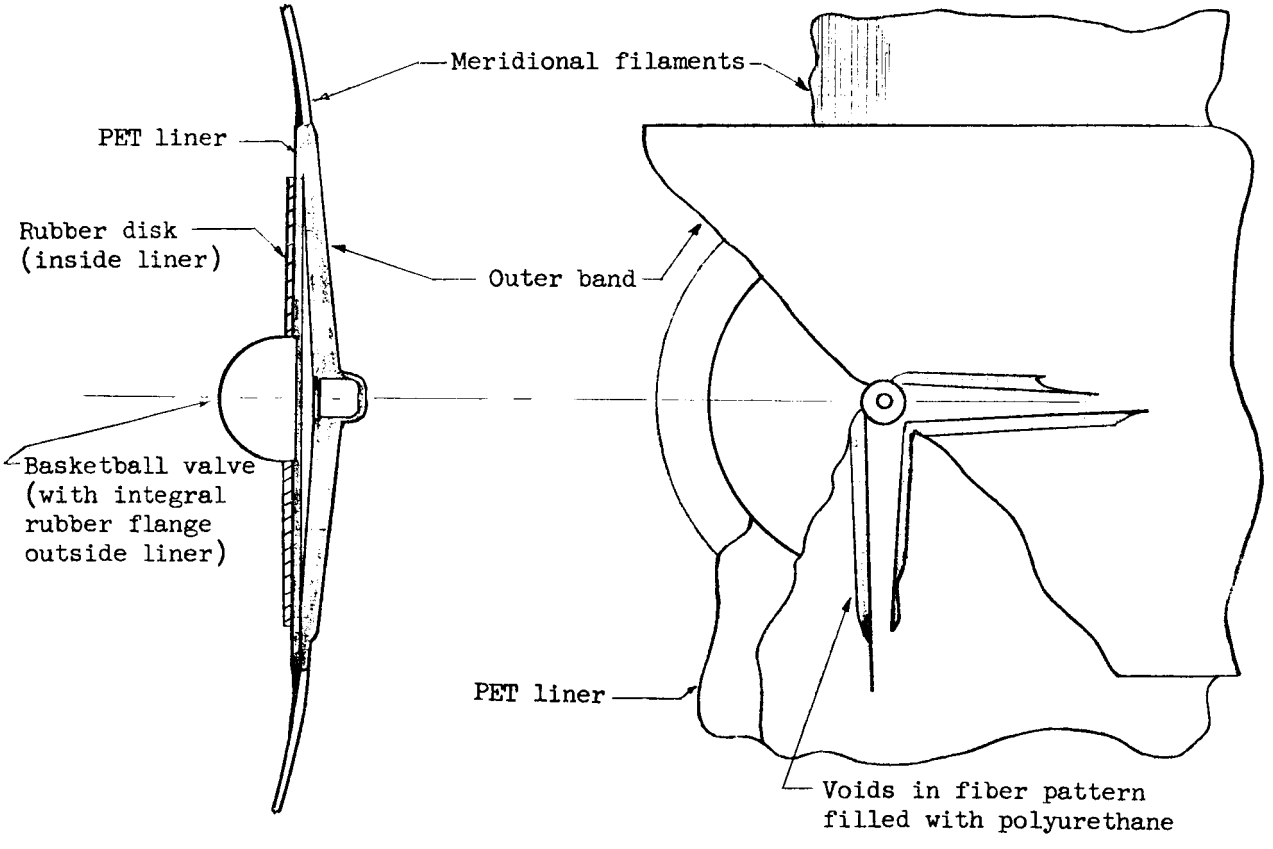

Figure 5.- Valve installation.

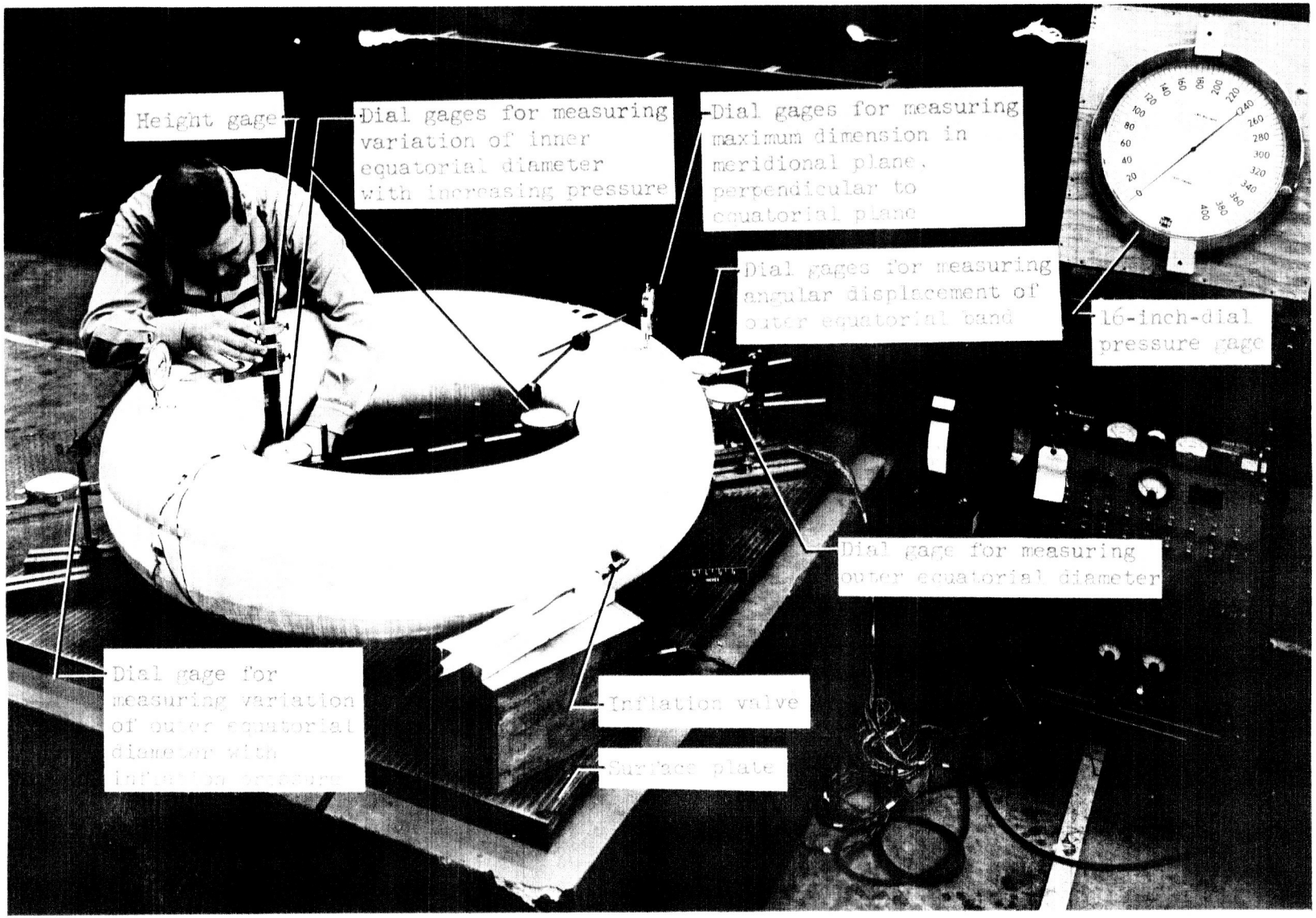

Figure 6.- Instrumentation used in dimensional stability tests. L-62-622.1

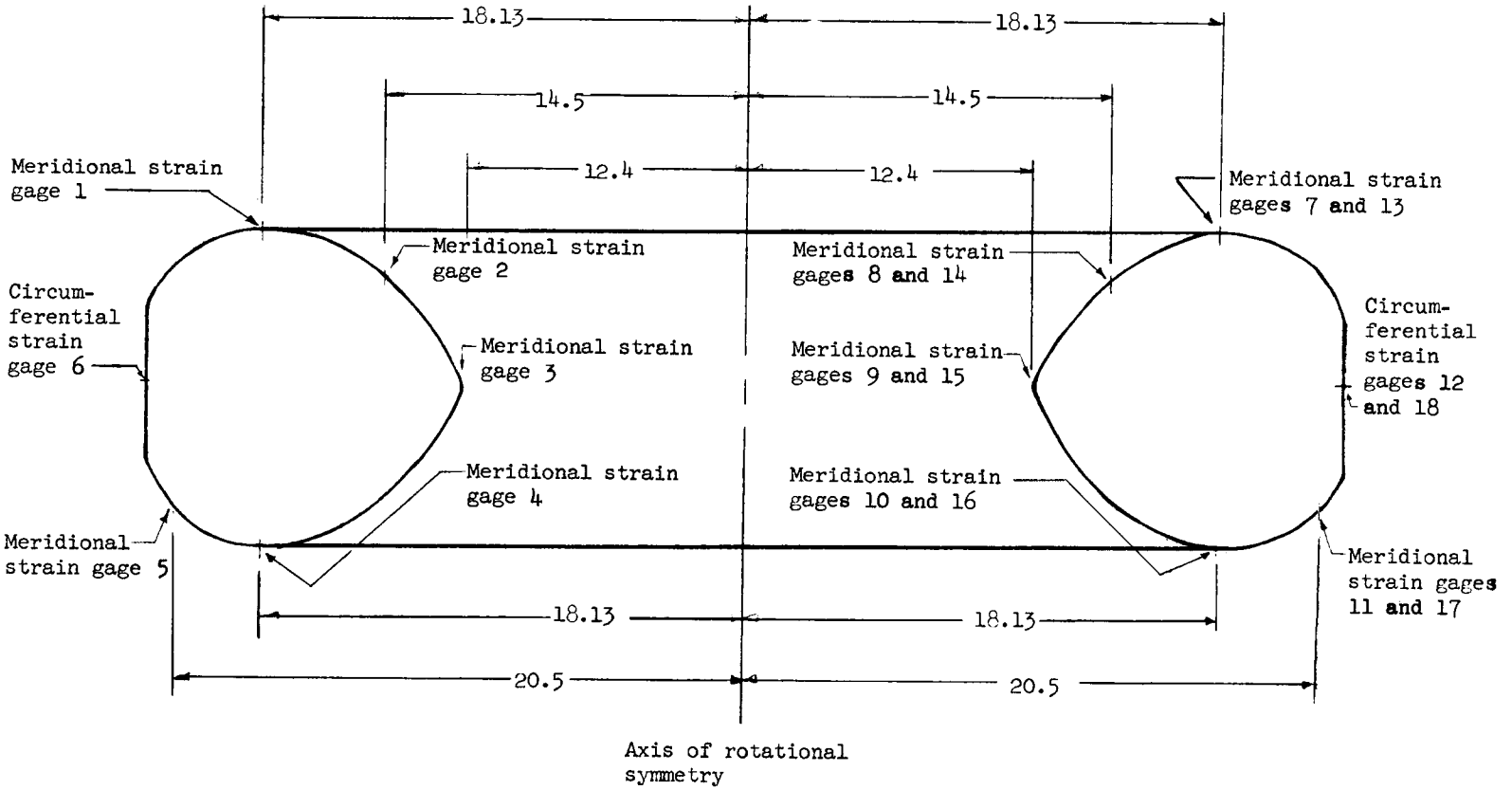

Figure 7.- Meridional plane cross-sectional view of 1/8-scale model showing strain-gage locations for load distribution test. Dimensions are in inches. (Gages 1 to 12 are regular foil gages and gages 13 to 18 are postyield gages.)

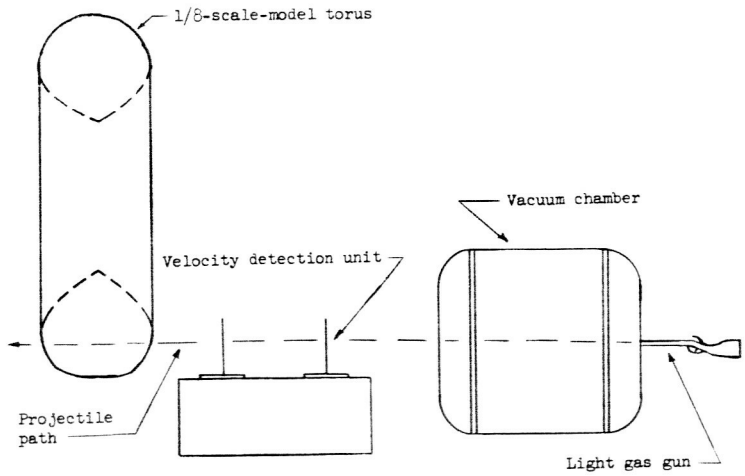

(a) Schematic of hypervelocity-impact test setup.

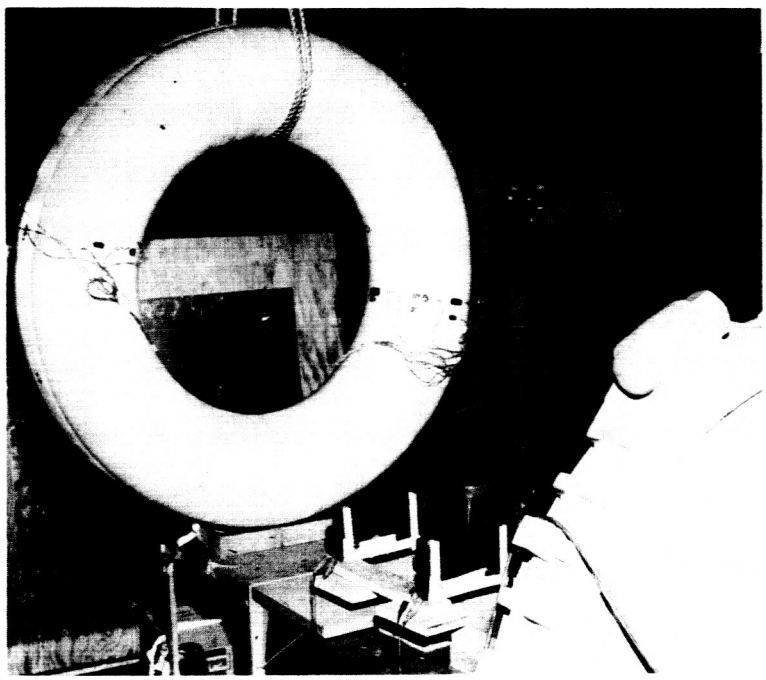

(b) Photograph of hypervelocity-impact setup. L-62-2205

Figure 8.- Instrumentation for 1/8-scale-model-torus hypervelocity-impact test.

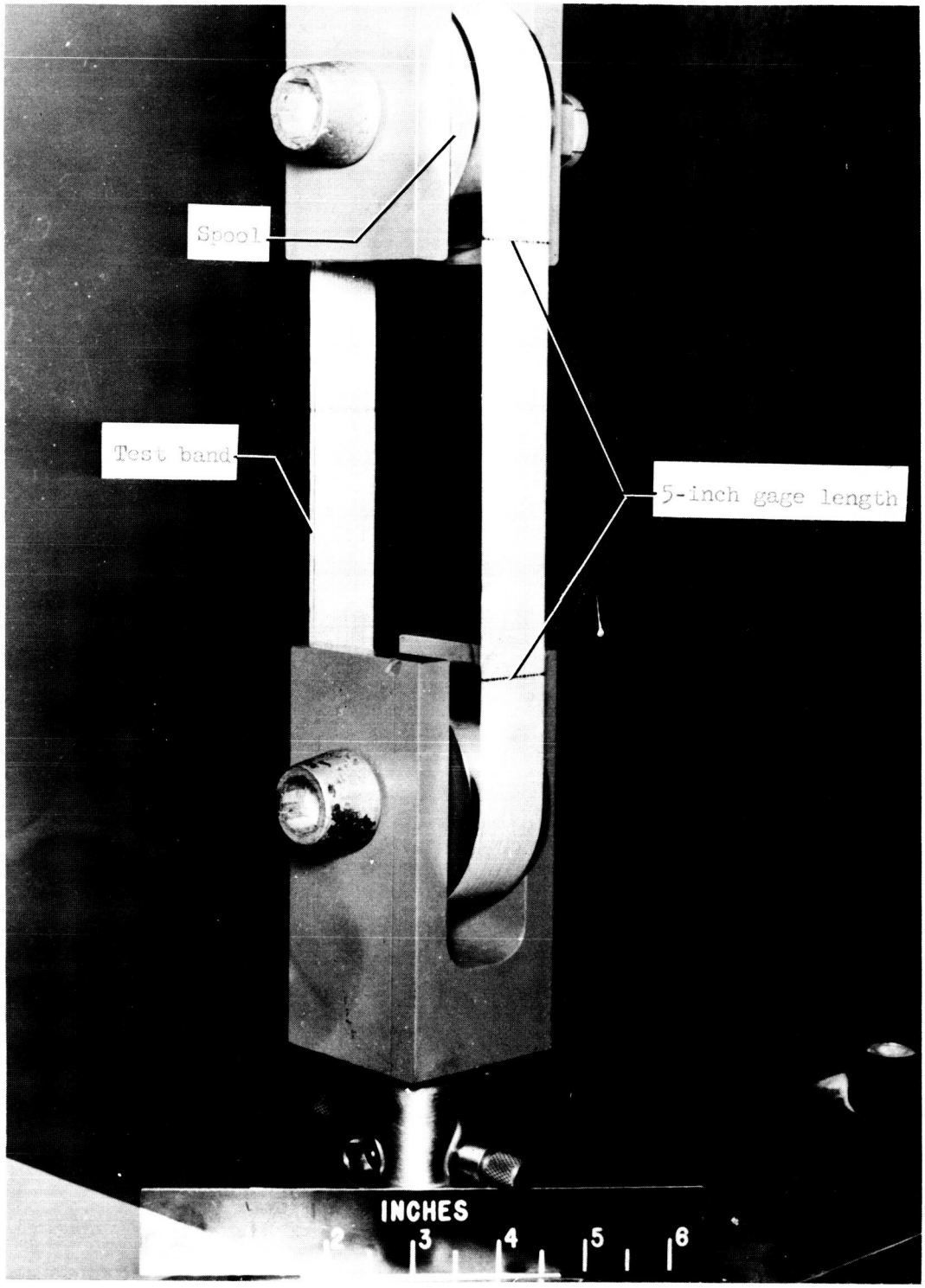

Figure 9.- Tension test band. L-62-3044.1

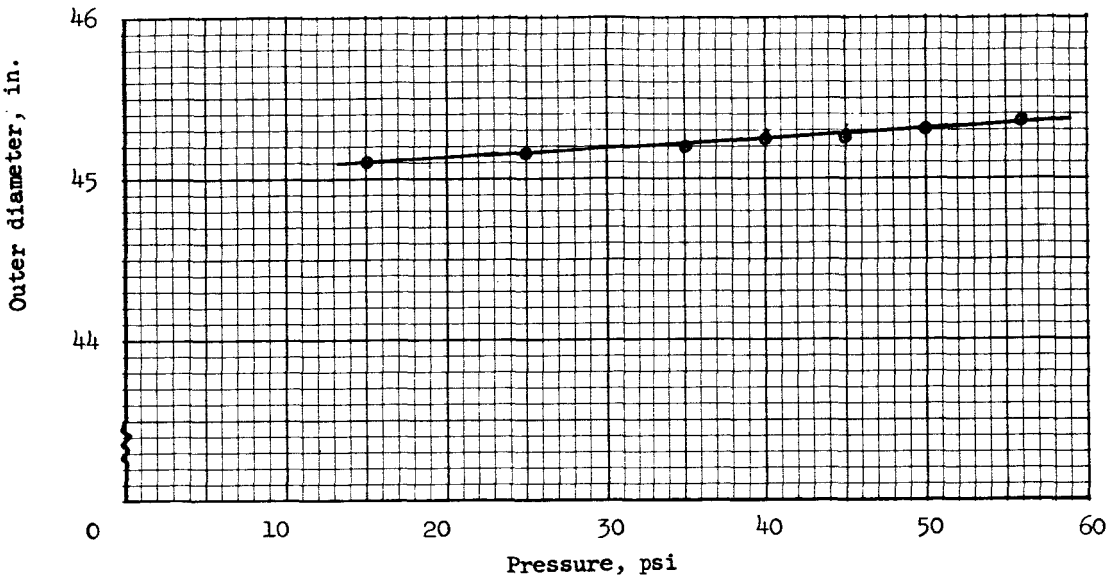

(a) Variation of outer equatorial diameter.

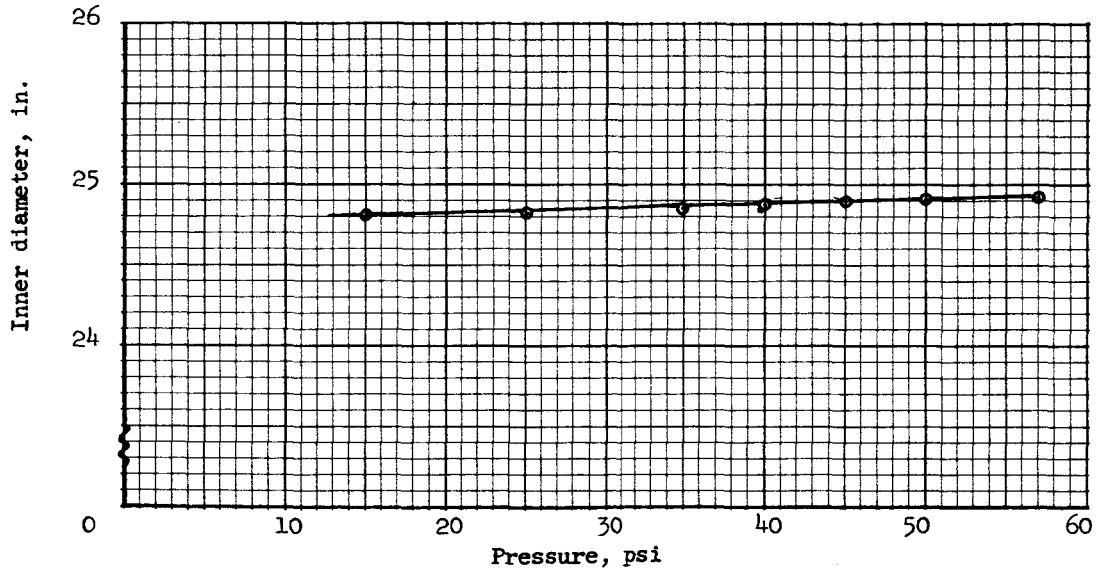

(b) Variation of inner equatorial diameter.

Figure 10.- Dimensional growth.

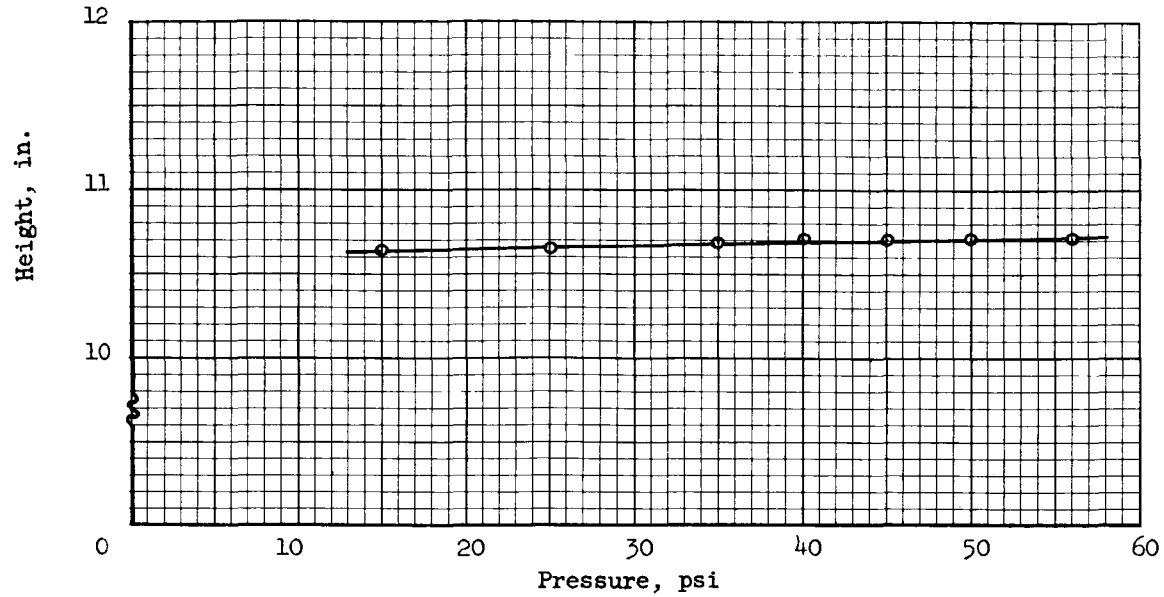

(c) Variation of height.

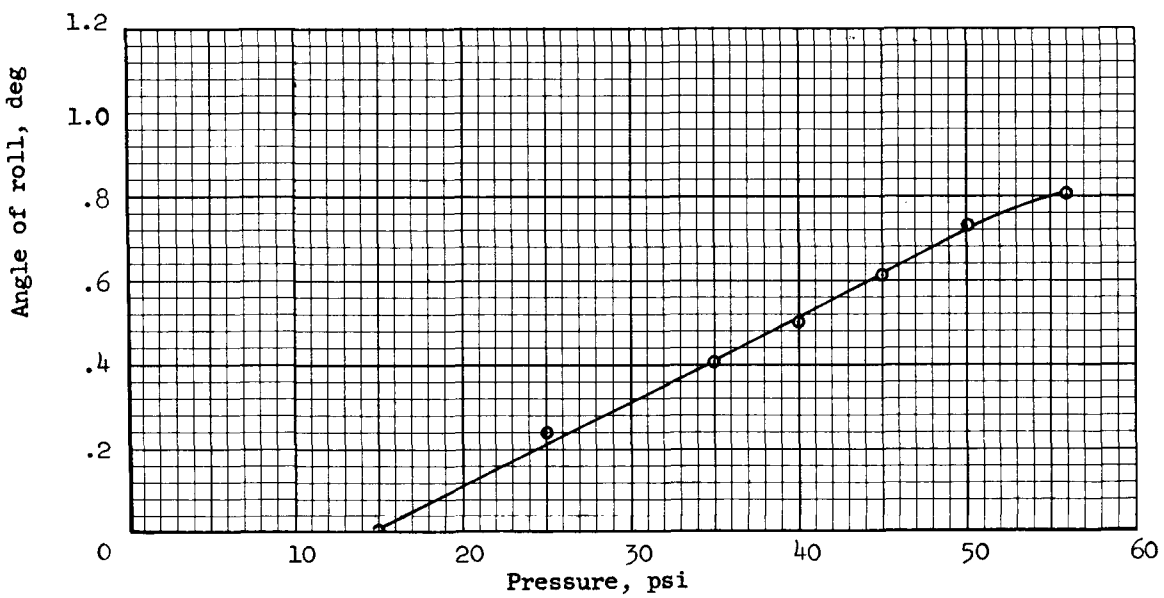

(d) Variation of angular displacement.

Figure 10.- Concluded.

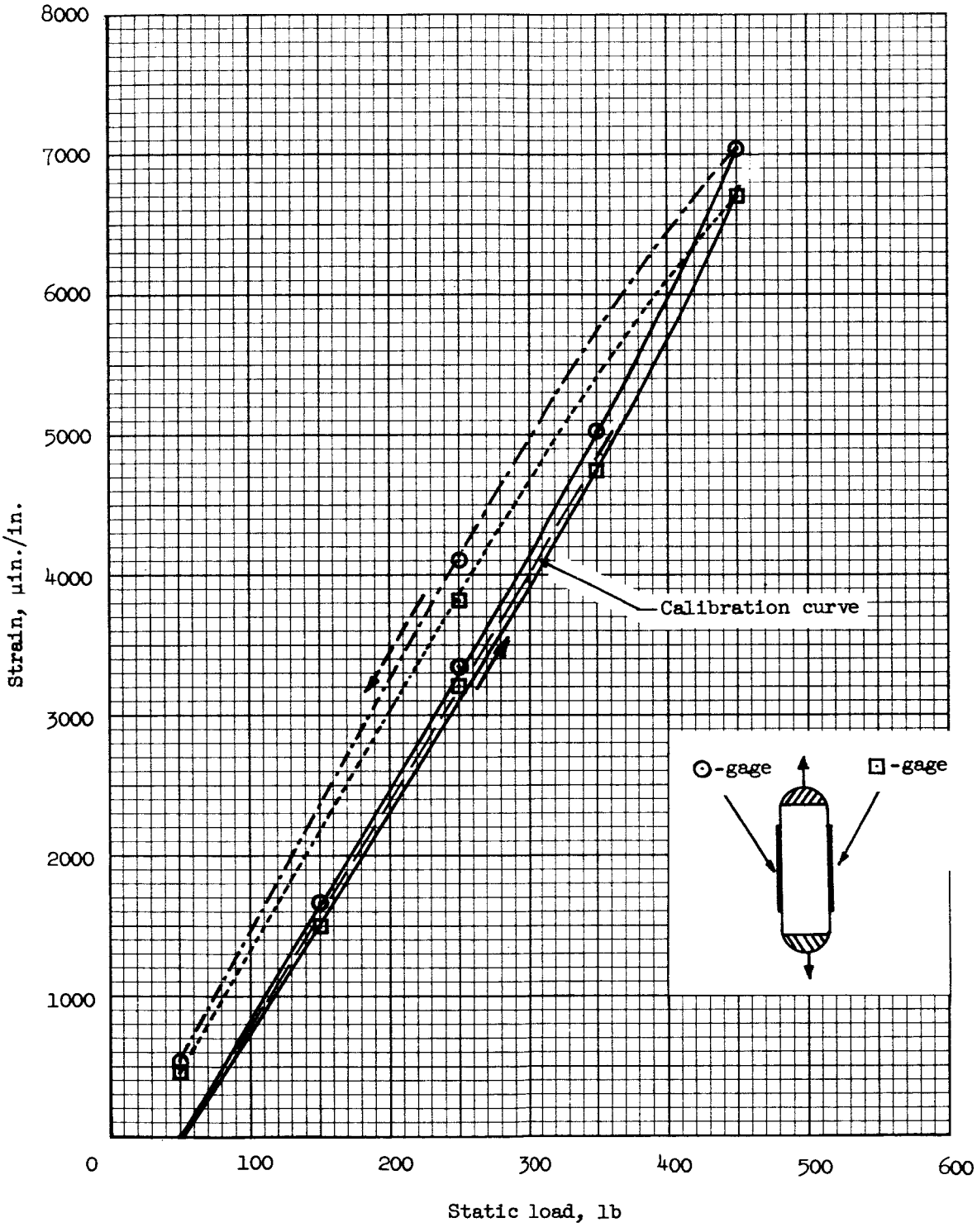

Figure 11.- Strain-gage calibration curve.

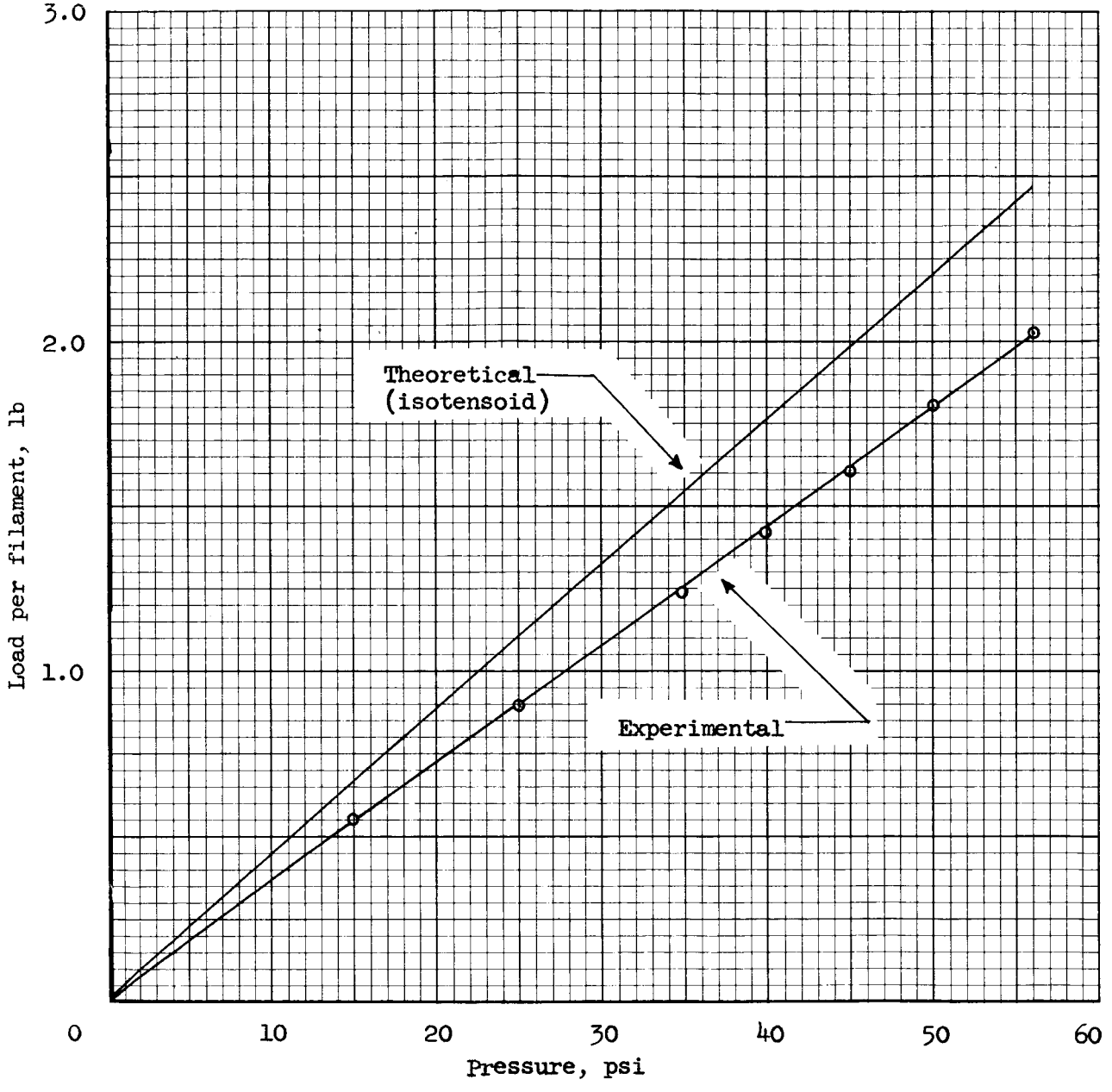

Figure 12.- Torus load per filament as a function of internal pressure for r_z = 18.13 in.

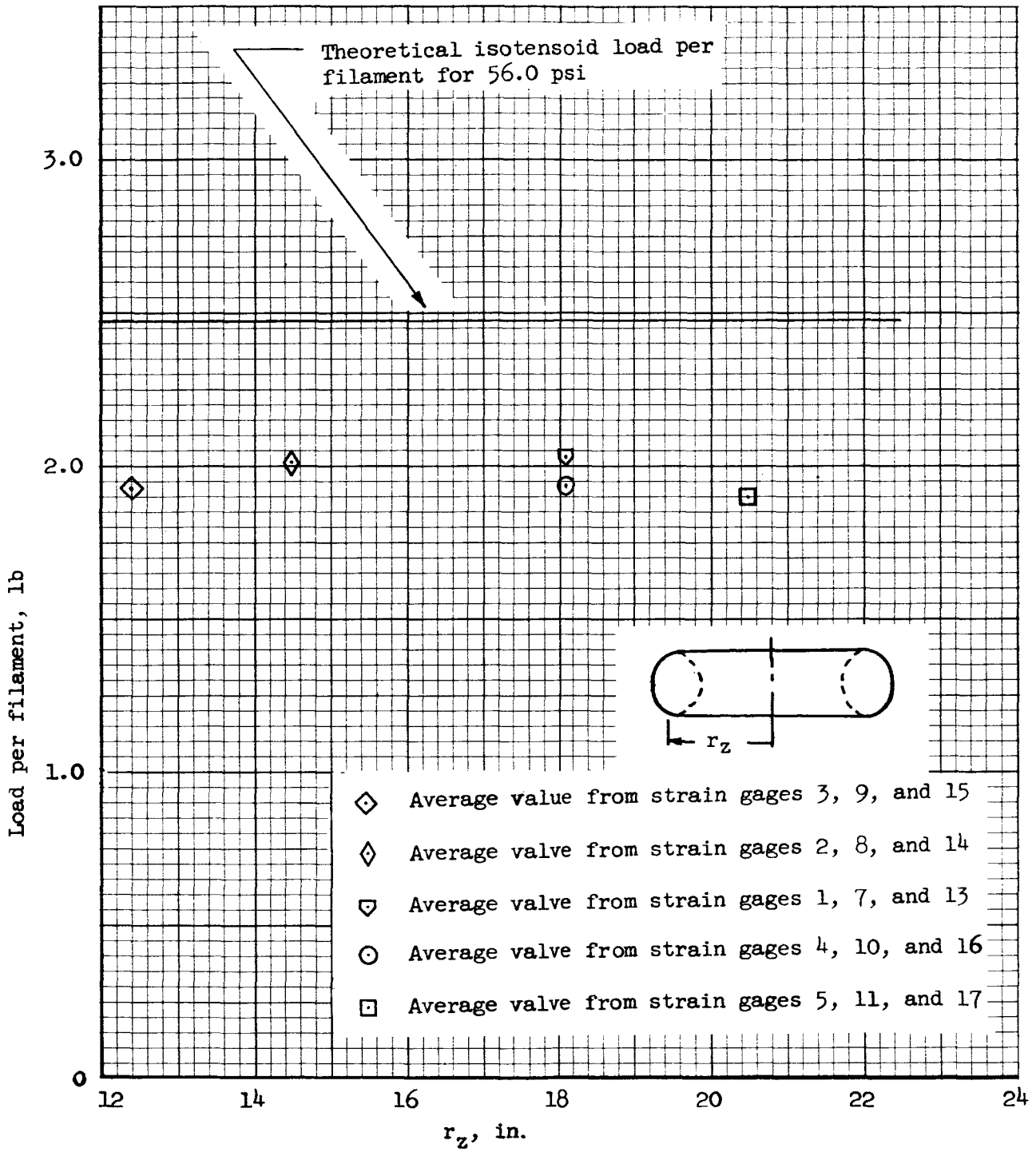

Figure 13.- Load per filament for an internal pressure of 56.0 psi.

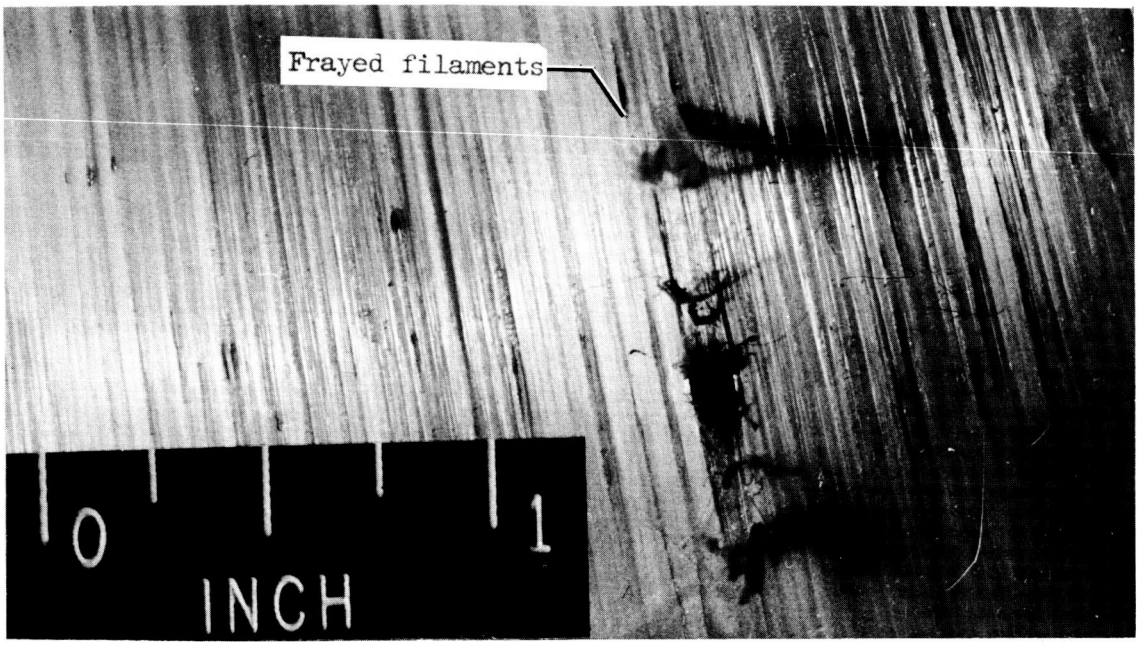

L-62-2206.1

(a) Exterior view of 1/8-scale-model torus showing projectile hole entrance.

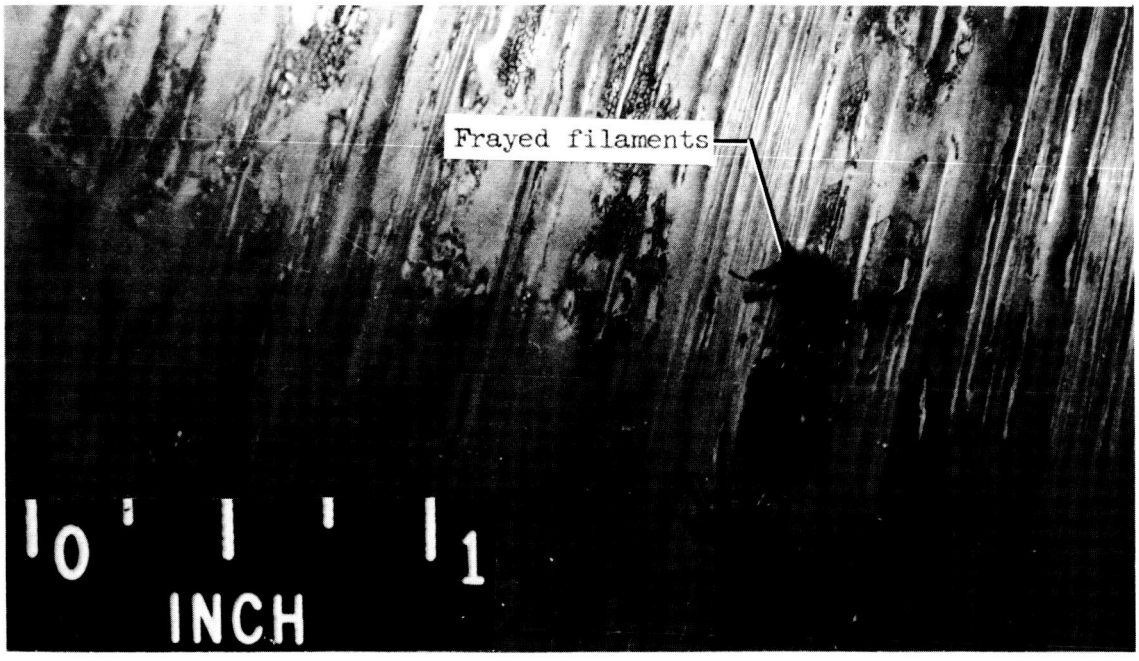

L-62-2207.1

(b) Exterior view of 1/8-scale-model torus showing projectile hole exit.

Figure 14.- Hypervelocity impact of 1/16-inch-diameter copper sphere into 1/8-scale-model torus.

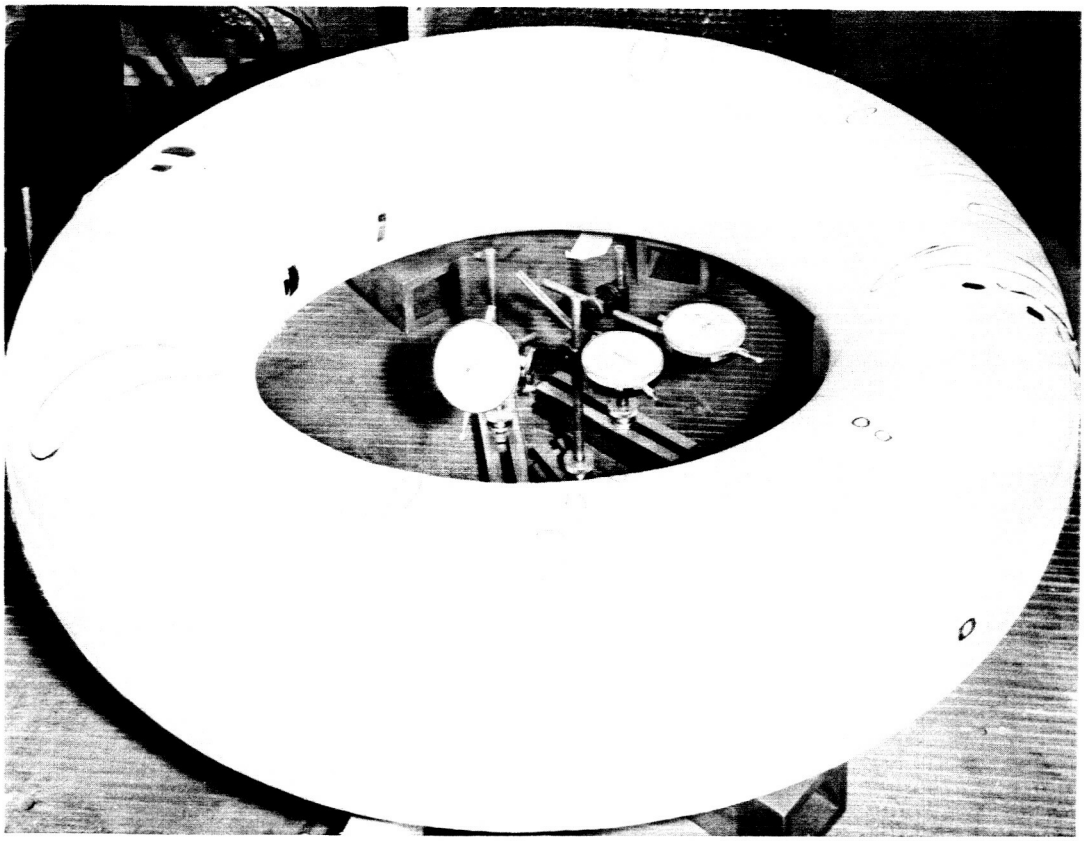

L-62-865

Figure 15.- The 1/8-scale-model torus after failure test. Circled areas indicate failure areas.

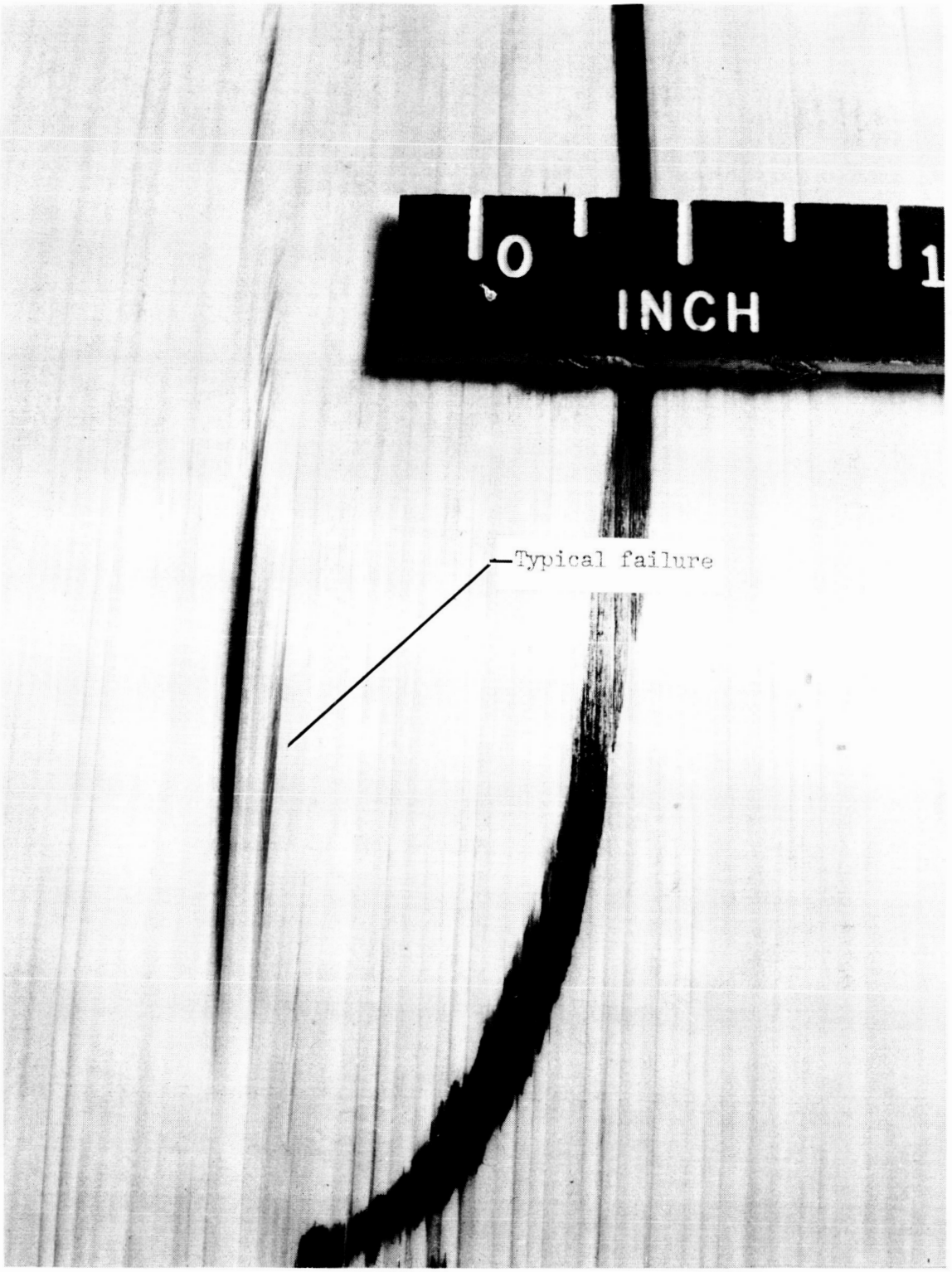

L-62-864.1

Figure 16.- Closeup of a typical structural failure.

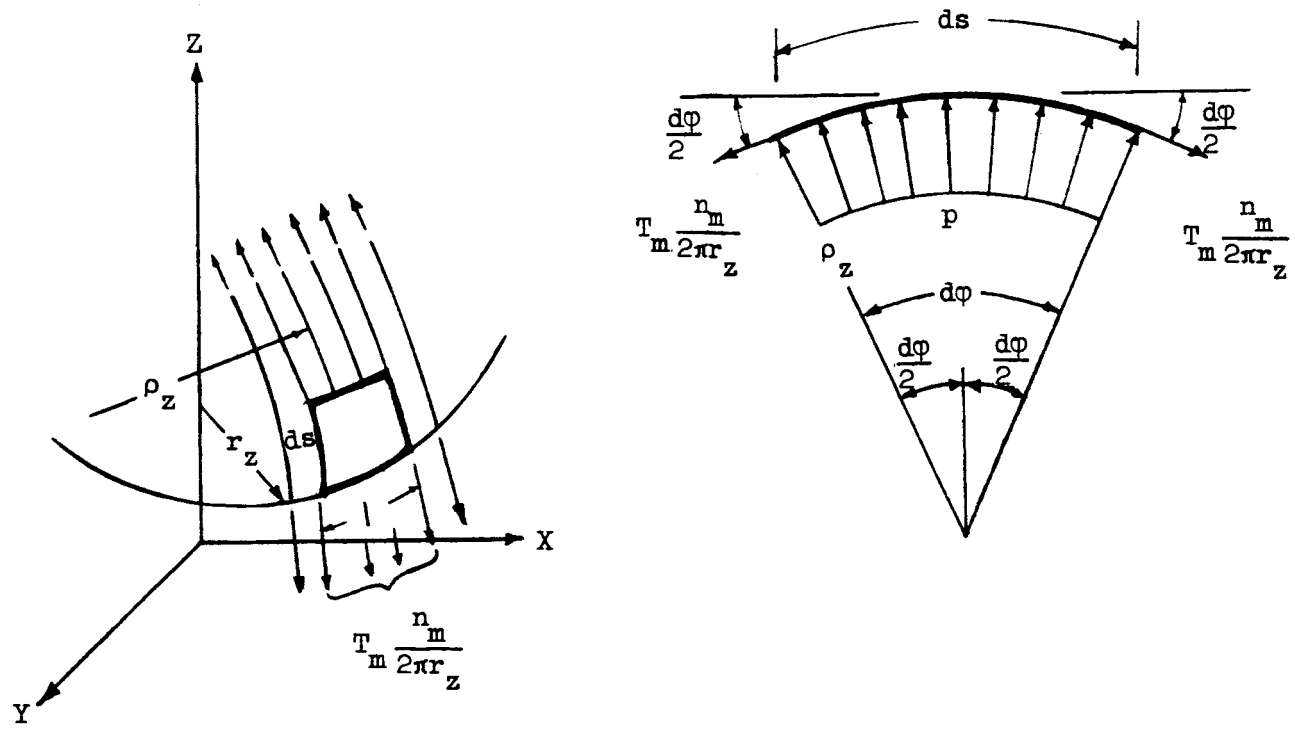

Figure 17.- Thin shell of revolution.

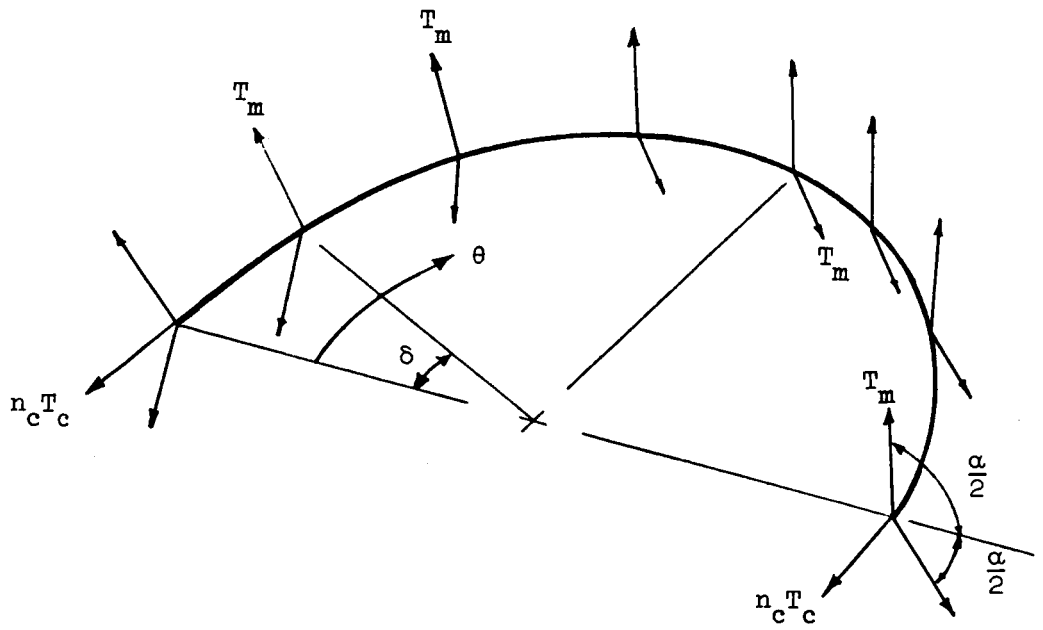

(a) Torus equilibrium.

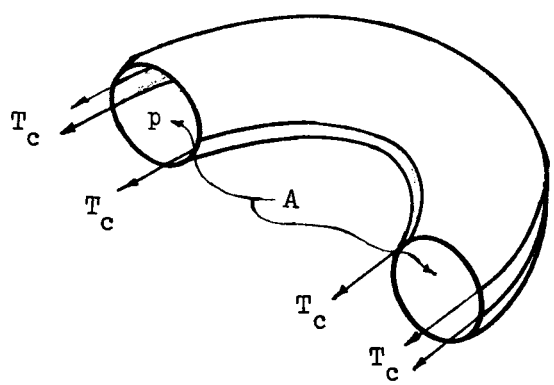

(b) Torus cross section.

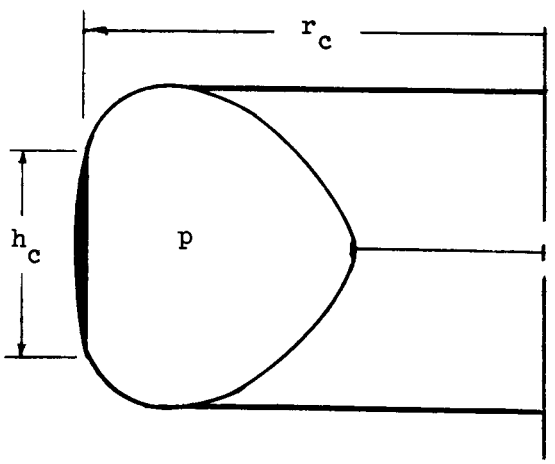

(c) Cross section, outer circumferential band.

Figure 18.- Torus circumferential band distribution.